POAC'23
Glasgow, United Kingdom

Proceedings of the 27th International Conference on
Port and Ocean Engineering under Arctic Conditions
12-16 June 2023, Glasgow, United Kingdom

Computational homogenization of an ice sheet with peridynamics

Wenxuan Xia[1], Erkan Oterkus[1], Selda Oterkus[1]

[1] PeriDynamics Research Centre, University of Strathclyde, Glasgow, UK

ABSTRACT

Ice-structure can form and evolve with complex internal arrangements. Factors such as granularity, porosity and crack formation can have a significant impact on the macroscopic structure response. Therefore, a multiscale analysis which applies a homogenization framework on the microscopic level can help capture the overall structure behaviour regarding microscopic structure defects. In this study, a peridynamic representative homogenization analysis is carried out on a semi-infinite ice plate with crack formed along the surface. Periodic boundary condition is applied around the representative volume element. Several homogenization analyses are performed with an increasing crack length, a decrease in corresponding effective elastic modulus is observed within the ice-structure.

KEY WORDS: Ice; Peridynamics; Homogenization; RVE.

INTRODUCTION

Ice sheet formed in natural settings can have complex internal structure. Factors such as granularity, porosity and internal crack distribution can have significant influence on overall ice-structure response and pose a challenge on computational modelling effort. To accurately predict the macroscopic response of an ice-structure, a microscopic structure analysis might need to be carried out. Current common multi-scale methods often utilize some form of computational approach within the realm of finite element method (FEM). Techniques such as extended finite element method (XFEM) and cohesive zone model (CZM) are suitable for solving crack propagation problems. However, FEM based methods require a sophisticated mesh generation scheme in order to adequately capture the crack propagation behaviour, thus introduces extra complexity and unknowns to the algebraic system which makes it difficult to be solved numerically.

Peridynamics is a new continuum mechanics formulation that is innate meshless, therefore mitigates the difficulties when dealing with structure non-linearity. Peridynamics formulation is non-local and contains no spatial derivatives, which makes it suitable for solving crack initiation and propagation problems. By implementing peridynamic analysis at microscopic

scale and link it towards the macroscopic FEM structure simulation, it creates a more effective approach when dealing with ice-structure interaction problems.

Many multiscale homogenization methods have been developed in the past, from simple rules of mixtures (ROM) approaches to more computational focused representative volume element (RVE) approaches. In general, RVE offers a versatile and reliable homogenization solution, which can be easily coupled with traditional FEM operation or peridynamic calculations. By introducing periodic boundary condition to the framework, peridynamic RVE analysis can offer a reasonable estimate towards the overall structure response when structural non-linearity is considered. Previous study saw the development of a bond-based peridynamic RVE approach for both 2-D (Xia, Oterkus and Oterkus, 2020) and 3-D (Xia, Oterkus and Oterkus, 2021a) settings. An ordinary state-based peridynamic RVE approach was also presented (Xia, Oterkus and Oterkus, 2021b). A non-ordinary state-based peridynamic homogenization framework was presented in a recent study by Galadima *et al*. (2022a). A comprehensive review of current peridynamic homogenization framework can be found in (Galadima *et al*., 2022b). In this study, a semi-infinite ice plate with crack is considered. Bond-based peridynamic RVE model is implemented to capture the decreasing effective material constants under the influence of a growing crack.

BOND-BASED PERIDYNAMIC FORMULATION

The equation of motion in peridynamics developed by Silling, S.A. (2000) and later generalized in Silling, S.A. *et al*. (2007) is a nonlinear integro-differential equation. As given in Madenci, E. and Oterkus, E. (2014)

$$\rho(\boldsymbol{x})\ddot{\boldsymbol{u}}(\boldsymbol{x},t) = \int_{H_x}[\boldsymbol{t}(\boldsymbol{u}'-\boldsymbol{u},\boldsymbol{x}'-\boldsymbol{x},t) - \boldsymbol{t}'(\boldsymbol{u}-\boldsymbol{u}',\boldsymbol{x}-\boldsymbol{x}',t)]dV' + \boldsymbol{b}(\boldsymbol{x},t) \quad (1a)$$

in which $\boldsymbol{u}$ and $\boldsymbol{u}'$ represent displacements of material points located at $\boldsymbol{x}$ and $\boldsymbol{x}'$, respectively. H_x defines the horizon of the material point located at $\boldsymbol{x}$ and its size is specified by the horizon size δ. The locality of interactions increases as δ decreases. Therefore, the classical theory of elasticity can be considered as a limiting case of the peridynamic theory as δ approaches zero (Silling, S.A. and Lehoucq, R.B., 2008). ρ, $\ddot{\boldsymbol{u}}$ and $\boldsymbol{b}$ represent density, acceleration, and body force, respectively. $\boldsymbol{t}$ and $\boldsymbol{t}'$ are peridynamic force density vectors between two material points.

Eq. (1a) can also be written in its discretized form given by Madenci, E. and Oterkus, E. (2014)

$$\rho(\boldsymbol{x}_k)\ddot{\boldsymbol{u}}(\boldsymbol{x}_k,t) = \sum_{j=1}^{N}\left[\boldsymbol{t}_{kj}(\boldsymbol{u}_j-\boldsymbol{u}_k,\boldsymbol{x}_j-\boldsymbol{x}_k,t) - \boldsymbol{t}_{jk}(\boldsymbol{u}_k-\boldsymbol{u}_j,\boldsymbol{x}_k-\boldsymbol{x}_j,t)\right]V_j + \boldsymbol{b}(\boldsymbol{x}_k,t) \quad (1b)$$

in which N is the total number of material points located within the horizon of the material point k and V_j represents the incremental volume of material point j.

As shown in Figure 1, material point k interacts with its family members within its horizon and is influenced by the collective deformation of all its family members, hence producing the force density vector $\boldsymbol{t}_{kj}$, acting at material point k. Likewise, material j is also influenced by the deformation of all material points within its horizon. The positions of material points k and j in the deformed state are specified by $\boldsymbol{y}_k = \boldsymbol{x}_k + \boldsymbol{u}_k$ and $\boldsymbol{y}_j = \boldsymbol{x}_j + \boldsymbol{u}_j$, respectively.

The equal and opposite pairwise force density vectors $\boldsymbol{t}_{kj}$ and $\boldsymbol{t}_{jk}$ satisfy the requirement for

balance of angular momentum, their expression is given by Madenci and Oterkus (2014) and can be written in discretized form as

$$\boldsymbol{t}_{kj}\left(\boldsymbol{u}_j-\boldsymbol{u}_k,\boldsymbol{x}_j-\boldsymbol{x}_k,t\right)=\frac{1}{2}C\frac{\boldsymbol{y}_j-\boldsymbol{y}_k}{|\boldsymbol{y}_j-\boldsymbol{y}_k|}=\frac{1}{2}\boldsymbol{f}(\boldsymbol{u}_j-\boldsymbol{u}_k,\boldsymbol{x}_j-\boldsymbol{x}_k,t) \tag{2a}$$

$$\boldsymbol{t}_{jk}\left(\boldsymbol{u}_k-\boldsymbol{u}_j,\boldsymbol{x}_k-\boldsymbol{x}_j,t\right)=-\frac{1}{2}C\frac{\boldsymbol{y}_j-\boldsymbol{y}_k}{|\boldsymbol{y}_j-\boldsymbol{y}_k|}=-\frac{1}{2}\boldsymbol{f}(\boldsymbol{u}_j-\boldsymbol{u}_k,\boldsymbol{x}_j-\boldsymbol{x}_k,t) \tag{2b}$$

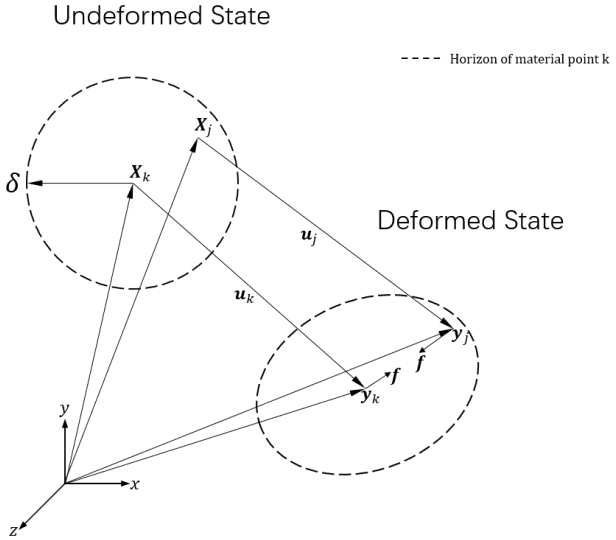

Figure 1. Deformed bond-based peridynamics configuration in comparison to its undeformed state and resulted pairwise equal and opposite force densities.

in which C is auxiliary parameters that depends on material constants, displacement field and horizon size. Substitute Equation 2 into Equation 1 produces the discretized bond-based expression of PD equation of motion at material point k as

$$\rho(\boldsymbol{x}_k)\ddot{\boldsymbol{u}}(\boldsymbol{x}_k,t)=\sum_{j=1}^{N}\boldsymbol{f}\left(\boldsymbol{u}_j-\boldsymbol{u}_k,\boldsymbol{x}_j-\boldsymbol{x}_k,t\right)V_j+\boldsymbol{b}(\boldsymbol{x}_k,t) \tag{3}$$

In which the force density expression $\boldsymbol{f}\left(\boldsymbol{u}_j-\boldsymbol{u}_k,\boldsymbol{x}_j-\boldsymbol{x}_k,t\right)$ can be assumed linearly dependent on the stretch between material points k and j as

$$\boldsymbol{f}\left(\boldsymbol{u}_j-\boldsymbol{u}_k,\boldsymbol{x}_j-\boldsymbol{x}_k,t\right)=cs(\boldsymbol{u}_j-\boldsymbol{u}_k,\boldsymbol{x}_j-\boldsymbol{x}_k,t)\frac{\boldsymbol{y}_j-\boldsymbol{y}_k}{|\boldsymbol{y}_j-\boldsymbol{y}_k|} \tag{4}$$

The definition for stretch $s(\boldsymbol{u}_j-\boldsymbol{u}_k,\boldsymbol{x}_j-\boldsymbol{x}_k,t)$ as given by Madenci and Oterkus (2014) can be written as

$$s\left(\boldsymbol{u}_j-\boldsymbol{u}_k,\boldsymbol{x}_j-\boldsymbol{x}_k,t\right)=\frac{|\boldsymbol{y}_j-\boldsymbol{y}_k|-|\boldsymbol{x}_j-\boldsymbol{x}_k|}{|\boldsymbol{x}_j-\boldsymbol{x}_k|} \tag{5}$$

The peridynamic bond constant, c depends on material constants and horizon size. Its expression for two-dimensional domain can be written as

$$c=\frac{9E}{\pi h\delta^3} \tag{6}$$

where E and h are the elastic modulus and thickness, respectively.

Material damage in peridynamics is represented by a bond failure parameter. If a bond passes

through a pre-existing crack or its stretch exceeds a critical value, the failure parameter will reduce the peridynamic force to zero, thus eliminating the interaction between those two material points.

PERIDYNAMIC RVE HOMOGENIZATION FOR SEMI-INFINITE ICE PLATE

RVE Model

For a sufficient sized representative volume element of a statistically homogeneous medium, computational homogenization can be performed to obtain a homogenized description for that medium.

The constitutive relations for the original heterogeneous material can be assumed as

$$\boldsymbol{\sigma} = \boldsymbol{C} \cdot \boldsymbol{\varepsilon} \tag{7a}$$

$$\boldsymbol{\varepsilon} = \boldsymbol{S} \cdot \boldsymbol{\sigma} \tag{7b}$$

$\boldsymbol{\sigma}$ and $\boldsymbol{\varepsilon}$ are the microscopic stress and strain field. $\boldsymbol{C}$ and $\boldsymbol{S}$ are stiffness tensor and compliance tensor, respectively.

Homogenization replaces the original heterogeneous material with a fictitious homogeneous medium

$$\bar{\boldsymbol{\sigma}} = \boldsymbol{C}^* \cdot \bar{\boldsymbol{\varepsilon}} \tag{8a}$$

$$\bar{\boldsymbol{\varepsilon}} = \boldsymbol{S}^* \cdot \bar{\boldsymbol{\sigma}} \tag{8b}$$

$\bar{\boldsymbol{\sigma}}$ and $\bar{\boldsymbol{\varepsilon}}$ are the macroscopic stress and strain field. Within a representative volume element, the macroscopic stress and strain field hold a constant value. $\boldsymbol{C}^*$ and $\boldsymbol{S}^*$ are effective stiffness tensor and effective compliance tensor.

where V is the volume of the representative volume element. According to average stress and strain theorem, the volume average of the stress or strain field inside the body is equivalent to the constant stress or strain tensor along the border, respectively, which can be expressed as

$$\frac{1}{V}\int \boldsymbol{\sigma}\, dV = \bar{\boldsymbol{\sigma}} \tag{9a}$$

$$\frac{1}{V}\int \boldsymbol{\varepsilon}\, dV = \bar{\boldsymbol{\varepsilon}} \tag{9b}$$

Substituting Equation 9a into Equation 8a gives

$$\boldsymbol{C}^* \bar{\varepsilon} = \frac{1}{V}\int \boldsymbol{\sigma}\, dV \tag{10}$$

in which the macroscopic strain $\bar{\boldsymbol{\varepsilon}}$ can be applied to a three-dimensional RVE as boundary conditions

$$\bar{\boldsymbol{\varepsilon}}_1{}^T = [c_s, 0,0,0,0,0] \tag{11a}$$

$$\bar{\boldsymbol{\varepsilon}}_2{}^T = [0, c_s, 0,0,0,0] \tag{11b}$$

$$\bar{\boldsymbol{\varepsilon}}_3{}^T = [0,0, c_s, 0,0,0] \tag{11c}$$

$$\bar{\boldsymbol{\varepsilon}}_4{}^T = [0,0,0, c_s/2\,, 0,0] \tag{11d}$$

$$\bar{\boldsymbol{\varepsilon}}_5{}^T = [0,0,0,0, c_s/2\,, 0] \tag{11e}$$

$$\bar{\boldsymbol{\varepsilon}}_6{}^T = [0,0,0,0,0, c_s/2] \tag{11f}$$

For a simplified two-dimensional RVE, the macroscopic strain $\bar{\boldsymbol{\varepsilon}}$ listed above is reduced to three loading cases with the third axis omitted from the equation. c_s represents a small scalar value controlling the magnitude of the macroscopic strain and can be chosen as $c_s = 0.001$ for later analysis.

To obtain the effective stiffness tensor $\boldsymbol{C}^*$ numerically, computational analyses can be carried out on RVE applied with boundary conditions listed in Equation 11. The effective stiffness tensor $\boldsymbol{C}^*$ is assembled column by column from the stress tensor $\boldsymbol{\sigma}$ obtained from the numerical analyses and the macroscopic strain $\bar{\boldsymbol{\varepsilon}}$ as

$$\begin{Bmatrix} C_{1,i} \\ C_{2,i} \\ C_{3,i} \\ C_{4,i} \\ C_{5,i} \\ C_{6,i} \end{Bmatrix} = \frac{1}{c_s} \begin{Bmatrix} \langle \sigma_i^{xx} \rangle \\ \langle \sigma_i^{yy} \rangle \\ \langle \sigma_i^{zz} \rangle \\ \langle \sigma_i^{yz} \rangle \\ \langle \sigma_i^{zx} \rangle \\ \langle \sigma_i^{xy} \rangle \end{Bmatrix}, \quad (i = 1,2,\dots,6) \tag{12}$$

where the angle bracket denotes volume average over RVE domain. For a simplified two-dimensional scenario, the effective stiffness tensor $\boldsymbol{C}^*$ is reduced to the size of three by three.

Apply Periodic Boundary Condition in Peridynamics

The macroscopic strain $\bar{\boldsymbol{\varepsilon}}$ can be enforced through several different implementations in peridynamics. It is possible to enforce Equation 11 periodically, as shown in Figure 2, several fictitious regions (labeled as 'child') are added surrounding the RVE. Several interior regions are also highlighted (labeled as 'parent') in order to establish a periodic displacement relationship.

The displacement value of a child point depends on the displacement value from its corresponding parent point. This periodic condition can be described by the following tensor notation

$$\boldsymbol{u}_i^c = \boldsymbol{u}_i^p + \bar{\boldsymbol{\varepsilon}}_{ij}(\boldsymbol{x}_j^c - \boldsymbol{x}_j^p) \tag{13}$$

In Equation 13, $\boldsymbol{u}$ is the displacement, superscripts c and p represent the corresponding child and parent point of every coupled material point-pair, as shown in Figure 2. $\boldsymbol{x}$ represent the location of a material point, and $\bar{\boldsymbol{\varepsilon}}$ is shown in Equation 11.

Decompose Equation 13 gives the displacement components of a child point as functions of their parent's displacement, relative location between point-pair and the strain scale c_s.

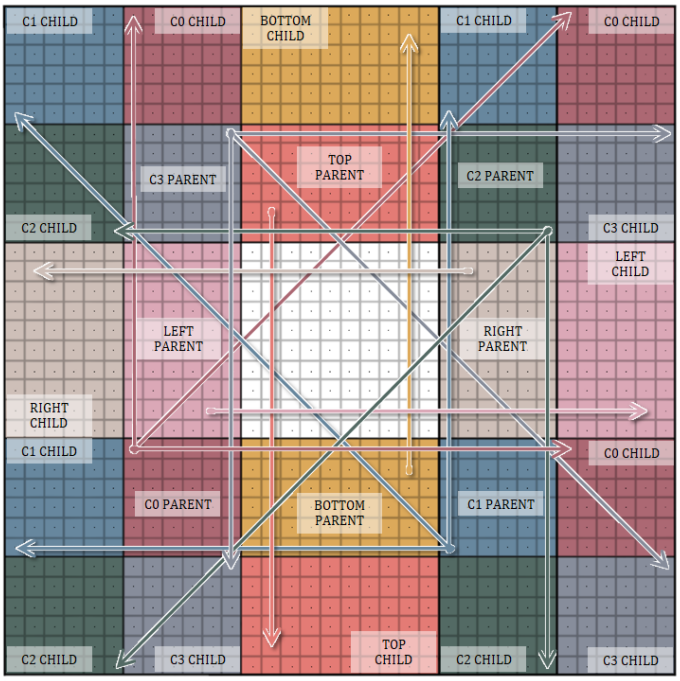

Figure 2. Peridynamic point coupling for periodic boundary condition.

Obtain Peridynamic Stress Tensor

The stress tensor $\boldsymbol{\sigma}$ in Equation 12 can be obtained from the displacement results of peridynamic analyses. As derived by Gu, Madenci and Zhang (2018), the peridynamic stress tensor $\boldsymbol{\sigma}$ can be expressed in terms of displacement gradient tensor $\nabla \boldsymbol{u}$, Elastic modulus E and Poisson's ratio v for linear isotropic material as

$$\boldsymbol{\sigma} = \frac{Ev}{(1+v)(1-2v)}[tr(\nabla \boldsymbol{u})]\boldsymbol{I} + \frac{E}{2(1+v)}[\nabla \boldsymbol{u} + (\nabla \boldsymbol{u})^T] \tag{14}$$

where $\boldsymbol{I}$ is the identity matrix.

The displacement gradient tensor $\nabla \boldsymbol{u}$ can be expressed as

$$\nabla \boldsymbol{u}_k = \left\{ \int_{H_k} \frac{\delta}{|\boldsymbol{x}_j - \boldsymbol{x}_k|} \left[(\boldsymbol{u}_j - \boldsymbol{u}_k) \otimes (\boldsymbol{x}_j - \boldsymbol{x}_k) \right] dV_j \right\} \boldsymbol{K}^{-1} \tag{15}$$

in which $\otimes$ denotes the dyadic product, $\frac{\delta}{|\boldsymbol{x}_j - \boldsymbol{x}_k|}$ is a scalar field acting as an influence function, and $\boldsymbol{K}$ representing the shape tensor

$$\boldsymbol{K}(\boldsymbol{x}_k) = \int_{H_k} \frac{\delta}{|\boldsymbol{x}_j - \boldsymbol{x}_k|} \left[(\boldsymbol{x}_j - \boldsymbol{x}_k) \otimes (\boldsymbol{x}_j - \boldsymbol{x}_k) \right] dV_j \tag{16}$$

Effective Elastic Modulus for Semi-Infinite Ice Plate with Crack

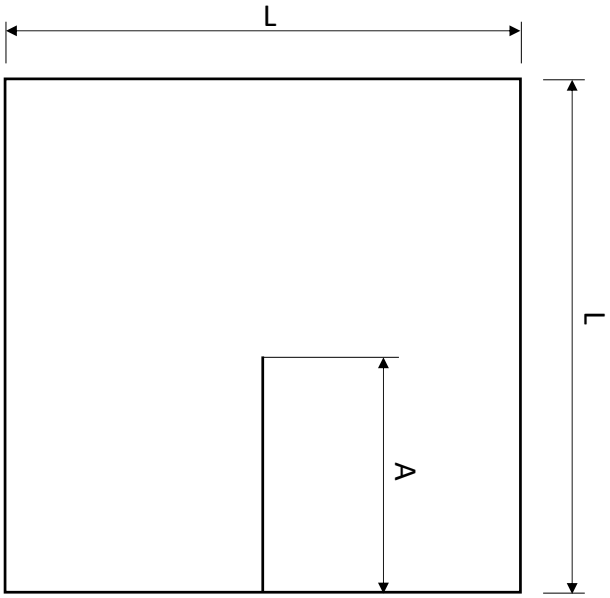

Figure 3. Semi-infinite ice plate with crack.

Consider a square semi-infinite ice plate with crack as shown in Figure 3. In order for the ice plate to be qualified as semi-infinite, its size L needs to be larger than four times its characteristic length (Vazic, Oterkus and Oterkus, 2020). Therefore, the size L is set to $L = 80\ [m]$, with Elastic modulus $E = 5\ [GPa]$ and ice thickness $t = 1.8\ [m]$.

For bond-based peridynamic analysis, the horizon size is set to $\delta = 3\ dx$ with $dx = 0.4\ [m]$. Poisson's ratio $v = 1/3$. A total number of 40000 peridynamic points are generated. Several crack sizes are considered where $A = 0, 10, 20, 30, 40\ and\ 50\ [m]$.

As demonstrated in (Xia, Oterkus and Oterkus, 2020) and (Xia, Oterkus and Oterkus, 2021b) for composite material and random crack inclusion, peridynamic RVE homogenization method can also be implemented in this semi-infinite ice plate scenario. Fictitious child points are added towards the exterior of the ice plate shown in Figure 3. Regions are created for periodic boundary condition as illustrated in Figure 2. Two-dimensional RVE homogenization analysis shows the effective elastic modulus E_{xx}^{*} decrease under vertical crack influence as shown in Table 1.

Table 1. Effective elastic modulus decreases under increasing crack influence.

A (m)	E_{xx}^{*} (GPa)	E_{xx}^{*}/E
0	5.00	1
10	4.86	0.97
20	4.48	0.90
30	3.94	0.79
40	3.34	0.67
50	2.72	0.54

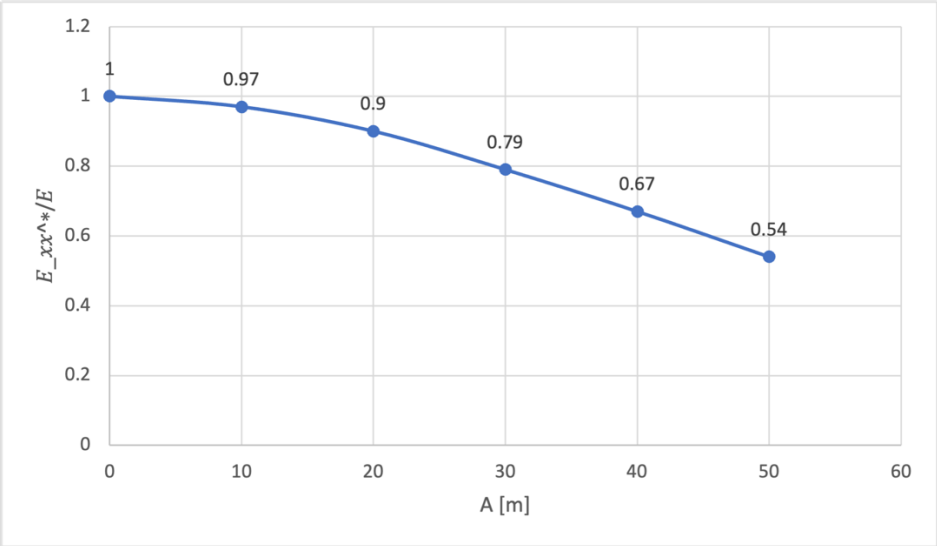

Figure 4. Effective elastic modulus decreases under increasing crack influence.

CONCLUSIONS

In this study, peridynamic RVE homogenization of a semi-infinite ice plate using periodic boundary condition is presented. Crack with various length is considered, where a decrease in horizontal effective elastic modulus is captured as the vertical crack increase in length. It can be seen from the result that peridynamic RVE homogenization can be used to predict effective material properties for semi-infinite ice plates with crack presence.

REFERENCES

Galadima, Y.K., Xia, W., Oterkus, E. and Oterkus, S., 2022a. Peridynamic computational homogenization theory for materials with evolving microstructure and damage. *Engineering with Computers*, pp.1-13.

Galadima, Y.K., Xia, W., Oterkus, E. and Oterkus, S., 2022b. A computational homogenization framework for non-ordinary state-based peridynamics. *Engineering with Computers*, pp.1-27.

Gu, X., Madenci, E. and Zhang, Q., 2018. Revisit of non-ordinary state-based peridynamics. *Engineering fracture mechanics*, 190, pp.31-52.

Madenci, E., Oterkus, E., 2014. *Peridynamic theory and its applications*. Springer, New York, NY.

Silling, S.A., 2000. Reformulation of elasticity theory for discontinuities and long-range forces. *Journal of the Mechanics and Physics of Solids* 48(1), 175–209

Silling, S.A., Epton, M., Weckner, O., Xu, J. and Askari, E., 2007. Peridynamic states and constitutive modeling. *Journal of Elasticity,* 88(2), pp.151-184

Vazic, B., Oterkus, E. and Oterkus, S., 2020. In-plane and out-of plane failure of an ice sheet

using peridynamics. *Journal of Mechanics*, *36*(2), pp.265-271.

Xia, W., Oterkus, E. and Oterkus, S., 2020. Peridynamic modelling of periodic microstructured materials. *Procedia Structural Integrity*, *28*, pp.820-828.

Xia, W., Oterkus, E. and Oterkus, S., 2021a. 3-dimensional bond-based peridynamic representative volume element homogenization. *Physical Mesomechanics*, *24*, pp.541-547.

Xia, W., Oterkus, E. and Oterkus, S., 2021b. Ordinary state-based peridynamic homogenization of periodic micro-structured materials. *Theoretical and Applied Fracture Mechanics*, *113*, p.102960.